Preferential Flow in Fractured Welded Tuffs

Rohit Salve

Earth Sciences Division
Lawrence Berkeley National Laboratory
Berkeley, CA

(Prepared for Water Resources Research)

Abstract

To better understand preferential flow in fractured rock, we carried out an *in situ* field experiment in the Exploratory Studies Facility at Yucca Mountain, Nevada. This experiment involved the release of ~22 m^3 of ponded water (at a pressure head of ~0.04 m) over a period of 7 months, directly onto a 12 m^2 infiltration plot located on a fractured welded tuff surface. As water was released, changes in moisture content were monitored along horizontal boreholes located in the formation ~19-22 m below. Distinct flow zones, with significant differences in flow velocity, size, and extent of lateral movement, intercepted the monitoring boreholes. Further, in some flow zones saturation levels persisted for the duration that water was released, while in others there were periodic fluctuations. There was also evidence of water being diverted above the ceiling of a cavity in the immediate vicinity of the monitoring boreholes. Observations from this field experiment suggested that inconsistencies exist in present conceptual models of flow in fractured rock. Particularly, these observations have shown that isolated conduits within the fractured rock formation encompass a large number of fractures to form preferential flow paths that persist if there is a continuous supply of water. It appears that in fractured welded tuffs, the propensity for vertical dispersion and fracture-matrix interactions may be significantly greater than suggested by existing conceptual models. An overriding conclusion is the need for field investigations at spatial scales of tens of meters to provide a fundamental understating of flow and transport in fractured, welded rock.

1. Introduction

Preferential flow in soils and fractured rock suggests channeling of flow through a subsection of the probable flow field. Such channeling is important to studies of flow and transport because it implies an accelerated movement of water and contaminants. In recent years, it has been of significant interest (and concern) to investigations that are evaluating sites for geological disposal of high-level nuclear waste, because of the potential for rapid movement of water to waste containers, and the migration of radionuclides that escape these containers.

Observations over the last 25 years from various field studies suggest that preferential flow is common in soils. In some of the earliest investigations, *Hillel and Parlange* [1972] found that a wetting front in coarse soils could become unstable, resulting in flow through "fingers." Subsequently, it was observed that preferential flow occurred in well-structured, loamy-to-clayey soils through cracks or fissures [*Beven and Germann*, [1982] . Recent studies suggest that preferential flow is usually caused by structural features (such as macropores), the development of flow instabilities within heterogeneous soil profiles, and the diversion of flow by sloping soil layers [*Simunek et al*., 2003]. However, preferential flow can probably also occur in relatively homogeneous media [*Roth*, 1995]

The evidence of preferential flow in fractured rock, though not as extensive as that for soils, includes a range of spatial scales and geological settings. For example, the Stripa Mine Test in Sweden, a tracer test conducted in fractured granite, identified a few relatively fast, isolated flow paths that transported tritium over a distance of 360 m in less

than 30 years, which was significantly faster than most of the water moving through the formation [*Abelin et al.*, 1991]. At Rainer Mesa, located ~200 km North of Las Vegas, Nevada, water was observed to seep into drifts several hundred meters below the ground surface, with only portions of the fractures transporting the water [*Thordarson*, 1965]. At the Idaho National Engineering and Environmental Laboratory (INEEL), an experiment to characterize flow in fractured basalt (which included an infiltration area of 6.5 acres) showed highly irregular water and tracer distribution with depth and time, suggesting the presence of multiple flow paths [*Wood and Norrell*, 1996]. In the Negev Desert, Israel, an investigation of flow and transport across a single fracture embedded in a 20-60 m thick zone of unsaturated chalk found infiltrating water to move along preferential flow paths, with only a small portion of the fracture plane controlling most of the activity [*Dahan et al*., 1998]. Observations of localized preferential flow have also been made at a much smaller scale in laboratory experiments that included flow along both natural rock surfaces and replicas [e.g. *Glass* 1993; *Nicholl et al.*, 1994; *Su et al.*, 1999; *Tokunaga and Wan*, 1997; 2001]. Despite the overwhelming evidence of preferential flow in soils and rocks, very little is known about the large-scale properties (e.g., structure, distribution, continuity) of such flow regimes. This information is important for predictive models, but it remains elusive, mainly because of the difficulties involved in characterizing flow that has substantial spatial (both vertical and horizontal) and temporal variability.

In this paper, we present the results from a field investigation, the broad objective of which was to study flow and transport in fractured welded tuff. Specifically, the goal for this effort was to identify and characterize flow paths that developed as water was released under ponded conditions along a 12 m^2 infiltration plot. Of particular interest

were features of flow paths such as flow velocities, size, spatial distribution, and temporal dynamics. We describe techniques used in the investigation, details of the observed flow paths, and conclude with a discussion about the important implications of the observations.

2. The Test Bed

The study was conducted in the Exploratory Studies Facility (ESF) at Yucca Mountain, which is ~160 km north of Las Vegas, Nevada (Figure 1a). Alternating layers of welded and nonwelded ash flow and air fall tuffs comprise the subsurface formations at Yucca Mountain [*Bodvarsson et al.,* 1999]. Closest to the surface is the welded Tiva Canyon tuffs, followed sequentially by the Yucca Mountain, Pah Canyon, and the Topopah Spring tuffs of the Paintbrush Group. The nonwelded tuffs of the Paintbrush group (PTn) lie immediately above the welded tuff of the Topopah Spring tuff (TSw), the host rock for this investigation. While no naturally occurring flow path has been observed at Yucca Mountain, there is some evidence that fast flow may have occurred along the ~ 600 m thick unsaturated zone between the ground surface and underlying water table. This includes the presence of perched water bodies with apparent ages younger than water in the surrounding tuff matrix [*Pruess et al.,* 1999], water-associated mineral deposits on some fracture surfaces [*Paces et al.,* 1996], and bomb-pulse ^{36}Cl signals detected at isolated locations within the mountain [*Fabryka-Martin et al.,* 1996].

The test bed extends from ~190 to ~215 m below the ground surface of Yucca Mountain. The upper and lower boundaries of the test bed were accessed through two tunnels, referred to as the Cross Drift and the Main Drift, respectively (Figure 1b). A

cavity, referred to as Alcove 8, was excavated into the walls of the Cross Drift. The floor of this cavity was used to introduce ponded water into the test bed (Figure 1c). A second cavity, referred to as Niche 3, was excavated into the walls of the Main Drift directly below Alcove 8, to permit access to the formation through boreholes used for monitoring flow and for visual observations of flow (Figure 1d).

The highly fractured, welded TSw found at this depth lies within a fairly homogeneous matrix [*Flint*, 1998] of moderately to densely welded ash-flow tuffs [*Hinds et al.*, 2003]. Alcove 8 is located within the Topopah Spring tuff upper lithophysal zone (Tptpul) [stratigraphic nomenclature of *Buesch* et al., 1996]. The Tptpul contains large naturally occurring cavities called lithophysae attributed to gas and vapor-phase constituents entrapped and redistributed during the initial deposition, compaction, and gas migration out of the TSw [*Buesch and Spengler*, 1998]. The majority of fractures appear to be cooling features associated with lithophysae cavities. Niche 3 is located within the Topopah Spring Tuff middle nonlithophysal zone (Tptpmn), which is a single cooling unit that formed about 12.8 Ma when a thick pyroclastic flow erupted from its volcanic sources. The Tptpmn subunit is a densely welded, highly fractured devitrified zone and contains few lithophysal cavities. There is a vertical distance of ~20 m between the floor of Alcove 8 and the crown Niche 3. The location of the Tptpul-Tptpmn contact is at ~3 above Niche 3.

3. Methods

To address the objectives of this investigation, water was released along the floor of Alcove 8 under ponded conditions for a period of approximately seven months. At

vertical distances of 19 and 22 m below the infiltration pond, an array of horizontal boreholes were instrumented with specially designed sensors to detect the arrival and persistence of flow through fractured rock.

3.1. Liquid Release along the Floor in Alcove 8

A 3×4 m^2 infiltration plot was located on the floor of Alcove 8 (Figure 2a). The boundary of the plot was made with steel sheets embedded into the floor. The plot was further divided into 12 square subplots, of similar size (i.e., 1 m^2). Each subplot was connected to a permeameter, designed to maintain the desired height of ponded water (i.e., ~0.02 m) while continuously monitoring the rate at which water was released into the infiltration plot. To minimize losses through evaporation, each infiltration subplot was covered with a plastic sheet, and the Alcove 8 cavity was isolated from ventilation effects in the Cross Drift by bulkhead doors.

The ponded infiltration test began on August 20, 2002, and continued until March 24, 2003, during which ~22,000 L of water was released into the test bed (Figure 2b). The daily infiltration rates rapidly increased to ~350 L/day during the first three weeks of ponding. This was followed by a more gradual decrease to ~75 L/day over the next six weeks. From this point onward, during the remaining 3.5 months, the infiltration rate dropped to ~40 L/day.

3.2. Monitoring of Flow in Fractures

Sensors to monitor saturation changes were installed in ten boreholes located in the immediate vicinity of Niche 3. Six of these boreholes, each 6 m long and originating along the walls of the niche, were oriented horizontally in a radial pattern into the formation around Niche 3 (BH1-6 in Figure 1d). A seventh borehole (BH7) was inclined

at a 30^0 angle upwards above BH4. Three additional boreholes (BH8-10 in Figure 1d), each 9 m long, were drilled ~1 m above the ceiling to run parallel to the central axis of the niche. All 10 boreholes had a diameter of 0.076 m. In BH1-7, BH9, and BH10, changes in saturation were recorded with electrical resistivity probes (ERPs), while psychrometers located along BH8 measured changes in water potentials during the entire investigation.

Salve et al. [2000] exploited the inverse relationship between resistance and saturation to develop the ERPs. The sensing element in the ERPs was a piece of filter paper across which changes in electrical resistance are measured (Figure 3a). The use of filter paper permitted a flexible sensing surface that could be molded to the contours of the borehole walls. These probes consisted of two electrical leads sandwiched between pieces of filter paper. To maintain a consistent geometry between probes, all electrical leads were cut to the same length and meshed through a nylon fabric, such that the distance between wires was the same for all sensors.

The core of the borehole monitoring system was a Measurement and Control System (MCS) [*Model CR7, Campbell Scientific Inc., Logan, Utah*]. To monitor a large number of sensors during field investigations, seven multiplexers [*Model A416, Campbell Scientific Inc., Logan, Utah*], each with a capacity to house 48 sensors, were attached to this unit. With this configuration, a sweep of 336 ERPs and 18 psychrometers could be made at 1-hour intervals. An internal check of the measurement system was continuously provided with precision resistors located randomly on the measurement ports of the multiplexers. Typically, the standard deviation from 1 KΩ and 100 KΩ precision resistor measurements were 0.001 and 0.005 KΩ, respectively.

The ERPs (in BH1-7, 9, and 10) and psychrometers (BH8) were housed in trays fabricated from 0.10 m OD PVC pipes cut lengthwise to produce a 0.075 m wide curved tray. On each tray, ERPs were installed at 0.25 m intervals along the outer surface, such that when the trays were located in boreholes, the probes were in direct contact with the borehole walls (Figure 3b). The psychrometers (in BH8) were located at 0.5 m intervals in small diameter holes (~ 3 mm ID) drilled through the PVC trays.

4. Observations

Twenty-nine days after water was introduced along the floor of Alcove 8, the first evidence of flow was detected ~20 m below, along BH9 (located ~ 1.0 m above the ceiling of Niche 3). At this time, ~6,000 L of water had been introduced into the infiltration pond (Figure 2b). Over the next 60 days, as an additional ~8,000 L of water entered the formation, wetting fronts were detected by ERPs at 24 locations along the 9 monitoring boreholes surrounding Niche 3. From the arrival time and location of the flow's leading edges , it appears that there were at least seven large flow paths (arbitrarily classified as being wider that ~1.0 m), and a few smaller distinct flow paths. In addition, sensors located close to the walls of the niche suggest that some water may have been diverted from the ceiling of the niche, possibly by capillary diversion. Table 1 summarizes the main features of each of the 24 wetting fronts and includes a grouping of the distinct flow paths. (Note that the flow paths identified will be referred to in the text as in Table 1, i.e., FP-A, FP-B, etc.). Figure 4 shows a plan and side view of the location of the wetting fronts and specific flow zones relative to the infiltration pond.

Among the flow paths that were detected, significant variability existed in the apparent velocity of flow (equated with the macroscopic linear distance divided by the arrival time), the wetting pattern associated with the leading edge of flow, size (along the horizontal plain), and location of the flow zone relative to the infiltration plot.

4.1. Large Flow-Path Features

The fastest observed velocities (i.e., 0.74 m/day) were measured along FP-A, located in the formation behind Niche 3. It included a section of BH4 and two sections along BH7, each ~0.50 wide and separated by a ~1 m wide dry zone that persisted during the entire period that water was released into the infiltration pond (Figure 5a). Along BH4, a ~0.75 m section of the borehole first wetted before the edge of flow spread horizontally over an additional 2.0 m during the next ~6 hours. Complete wetting (as suggested by constant low resistance measurements) occurred at each location as soon as the wetting front arrived. Similar wetting trends were observed along two sections of BH10 that were intercepted by two distinct flows. Since the end of BH 4 is at a horizontal distance of 6.25 m from the nearest edge of the infiltration plot, this flow zone had significant lateral movement as it traversed the ~22 m vertical distance from the infiltration plot to the BH4 and BH7.

FP-B, which was also located immediately behind the end of Niche 3, intercepted BH4, B9, and BH10 (Figure 4a). The ERP response suggests that a ~1.5 m wide flow path intercepted BH10 almost instantly before traveling towards BH4 (Figure 5b). The velocity of the wetting front for this flow ranged between 0.64 and 0.69 m/day as it migrated a distance of ~2.4 -3.8 m from the edge of the infiltration pond.

FP-C was detected along BH2, as a single continuous wet zone 46 days after ponded infiltration began. The pattern of wetting (more diffuse than sharp) along this ~2.5 m section of borehole suggests that the wetting edge moved slower here than in the faster flow paths (e.g. FP-A and FP-B), which were defined by a sharp change in measured resistance (Figure 5c). Here, the wetting began close to the borehole collar before migrating 1.75 m horizontally towards the midsections of the borehole over a period of ~108 hours. Wetting associated with this flow was slow, with saturations gradually increasing over a period of up to 5-10 days.

Flow associated with FP-D was almost as wide at the section of FP-A intercepted by BH4. This flow zone was located vertically below the infiltration pond and extended over a distance of ~2.0 m along BH10 (Figure 5d). However, despite being the flow path closest to the infiltration pond (because of the absence of lateral flow), the flow velocity measured along this zone (i.e., 0.43 m/day) was significantly less than that measured in most other locations.

FP-E was one of two distinct flow paths that intercepted BH3. This flow was detected along the mid-section of BH3 and had an initial velocity of 0.40 m/day (Figure 6). It was located between 3.15 and 3.90 m from the edge of the infiltration pond. The response of the ERPs suggests that the wetting front intercepted BH3 at a distance of 3.15 m from the collar, after which horizontal wetting progressed ~1 m deeper into the borehole over a period of at least one week.

FP-F was the last flow path detected in the boreholes surrounding Niche 3. This flow path intercepted a section of BH6 ~91 days after the start of infiltration in Alcove 8, and 60 days after the first flow path (i.e., FP-A) intercepted BH9. The horizontal spread

of flow was similar to the section of FP-A intercepted by BH4. However, unlike BH4, where the wetting front intercepted the borehole almost instantly, wetting along the 2.75 m section of borehole BH6 continued for more than nine hours.

4.2. Flow Close to Niche Walls

In six of the seven boreholes extending from the walls of Niche 3 (i.e. BH2-BH7), wetting was observed close to the niche walls (Figure 7). In five of these (BH3-BH7), saturations increased to a limited horizontal distance (i.e., 0.50 m), while in the single exception (i.e., BH2), the wetting phase extended ~2.5 m horizontally. Further, periodic observations made along the walls of Niche 3 show the emergence of water through a network of fractures (Figure 8).

The first of these flows was detected along BH7 located at the back of Niche 3, 33 days after the ponded infiltration experiment started. Two days later, BH4 (located immediately below BH7) detected flow at similar distances from the Niche 3 wall. Along BH2 and BH3, wetting occurred close to the wall almost simultaneously, 45 days after the start of ponding. Fifteen days after BH3, flow close to the walls of Niche 3 was detected along BH6, and then two days later along BH5.

From the pattern of wetting, timing, and location of these flows, it appears that moisture detected in BH2 and BH3 likely traveled relatively fast close to the niche wall, before moving at a relatively slower rate deeper into the formation. This is suggested by the rapid drop in resistance measured by the sensors located 0.15 m from the collars of the two boreholes and the delayed, more gradual decrease in resistance observed in the sensors located 0.40 m from the collar in both boreholes. It is possible that this wetting pattern is the result of flow diversion occurring above the Niche 3 ceiling close to the

location of BH8 (Figure 4). (Flow was not detected along this borehole because it was not instrumented with ERPs.)

At the other locations, wetting appears to have started further into the formation before migrating towards the niche wall. It is likely that flow detected near the collars of BH4 and BH7 is part of the FP-B, while flows detected near BH5 and BH6 are from FP-D, which was initially intercepted by BH10.

4.3. Persistence of Flow Paths

Flow paths intercepted by monitoring boreholes 30-90 days after the start of the infiltration experiment persisted during the next few months as the ponded release of water continued in Alcove 8. However, following initial wetting, the response to the continuous release of ponded water varied significantly along the some flow paths.

Along wetted sections of BH4 and BH7 associated with FP-A and FP-B, saturation levels remained, for the most part, unchanged following the establishment of flow zones. Within these flow zones were a few discrete points in which there was gradual continuous drying or wetting (Figure 9a). Similar observations of discrete locations showing wetting and/or drying were also observed in BH2 and BH3.

At the terminal section of BH10 intercepted by FP-B, significant variability occurred in saturations levels along a portion of the flow zone (i.e., between 6.65 and 7.15 m) during the duration of the ponded infiltration (Figure 9b). Here, following initial wetting (31 days after the start of water release along the infiltration zone), there was a period of ~45 days during which there was gradual drying, followed by an abrupt wetting event. Near-constant saturation levels for the subsequent two weeks indicate that wetting persisted along this zone before it began to dry again over the next 30-45 days. Following

this period of drying, the zone again began to wet gradually until the end of the monitoring period.

Along FP-F, located along the midsection of BH6 (which was the last flow zone detected by the monitoring boreholes), three episodes of rapid wetting and rapid drying occurred during the infiltration experiment (Figure 9c). Immediately after the wetting front intercepted BH6 for the first time, 91 days after start of ponding, the wet zone began to dry over a period of 10 days, after which saturation along the wet zone remained constant for the next three weeks. This section of borehole then wetted again briefly, before drying over the next two days. Two weeks later, a third wetting front occurred, during which higher saturations persisted for almost three weeks before there was some drying.

These observations show that generally, flow zones detected earliest in the boreholes around Niche 3 remained persistent during the infiltration period, while the slower flows were subject to periodic changes in saturations. It appears that the slower flow zones were significantly transient, with flows periodically increasing and decreasing even as the ponded release of water persisted.

5. Discussion

This study was conducted within the ~150 m thick TSw unit, which is likely to host a large portion of the potential repository at Yucca Mountain [*McKenzie*, 1999]. Within the TSw, ~300 m below the crest of the mountain, a series of underground openings called drifts will be constructed in which to place containers of radioactive waste.

In the prevailing conceptual models of unsaturated flow at Yucca Mountain, water infiltrating the surface results in flow paths along fractures within the TSw. A key input in the assessment of subsurface flow and transport by numerical models has been the properties of fractures, which include fracture connectivity, fracture permeability, fracture porosity and fracture-matrix interactions [*Hinds et al.*, 2003]. These properties have been derived from fractures mapped to have trace lengths greater than a meter. The majority of fractures (i.e., those with trace lengths of less than one meter) have for the most part not been considered in these models. As a result, fractures in conceptual and numerical models of flow in the TSw are spaced at ~0.5 m intervals [*Beason,* 1996], with flow assumed to occur at ~10 m intervals [*Hinds et al.*, 2003].

Other conceptualizations have suggested that under ambient conditions, only a small portion of the fractures in the TSw actually carry water, with flow focusing occurring because of mechanisms such as fracture heterogeneity and gravitational instabilities [*Liu et al.,* 1998]. Consequently, the matrix surface area in contact with percolating water in an active fracture (i.e., a fracture that transmits water) is thought to be limited because of this gravitational flow fingering [*Hinds et al.,* 2003]. It is further assumed that in the immediate vicinity of the drifts, water percolating from the unsaturated zone above may be retarded by capillary barriers at the drift ceiling, thereby preventing the water from dripping to the drift (Trautz and Wang, 2002).

A prominent feature of this investigation was the interception and characterization of numerous flow zones as a flow field developed during the ponded release of water into fractured rock. (This prescribed upper boundary represents a condition that could prevail at the PTn-TSw interface, with water flowing down a fault embedded in the PTn into the

fractures of the TSw.) To our knowledge, these preliminary insights into specific flow zone features in unsaturated fractured rock have not been observed in previous studies at this spatial and temporal scale.

Some of the water released into the formation under a positive head (i.e., 0.04 m) at Alcove 8 was intercepted by the monitoring boreholes located ~19-22 m vertically below, and at a horizontal distance of between 0 to 4.75 m from the boundaries of the infiltration pond. While the maximum horizontal distance between intercepted flow zones was ~9 m (FP-E and FP-A), multiple flow zones were observed along some of the 6 m monitoring boreholes (Figure 6). Further, the location of distinct flow zones intercepted along the horizontal plain surrounding Niche 3 suggests that some divergence occurred as water moved vertically through the test bed. Within Yucca Mountain, where the TSw extends, on average, ~150 m vertically [*Bodvarsson et al.,* 2003], the lateral spread of water resulting in flow along preferential flow paths could be significant.

Despite evidence of lateral movement of water, it is not apparent where this diversion was initiated along the test bed. As gravity-dominated flow proceeds in a generally downward direction, lateral broadening is thought to occur because of capillary effects, which are exacerbated by dispersion effects from random medium heterogeneities [*Pruess*, 1996]. From the wetting patterns associated with the front edge of each flow zone, it appears that lateral broadening may have occurred along BH2, where there was a clear temporal trend to wetting along the horizontal. For the majority of flow zones, however, distinct wet zones separated by dry zones suggest that the movement of water towards Niche 3 was along well-defined preferential flow zones (with minimal lateral broadening) that intercepted the infiltration plot. This corroborates the observations from

the flow and transport experiment in the Stripa Mines, in which distinct isolated channels of flow were observed in the fractured granite formation [*Abelin et al.,* 1991].

Possible divergence of flow resulting from capillary barrier effects (corresponding to the Niche 3 cavity) is suggested from the response measured in at least two boreholes (BH2 and BH3 in Figure 7), which showed fast wetting along the formation close to the niche wall. However, the effectiveness of a capillary barrier in reducing the amount of water entering the excavated cavity may be minimal, because much of the water diverted to the side walls is able to move towards the cavity from other locations, especially at breaks in the capillary barrier (Figure 8). Observations from this investigation show that it is possible for a cavity surrounded by fractured rock to redistribute water from the ceiling to the side walls, thereby increasing the area through which water can enter the niche.

The nearly instantaneous wetting of individual wet zones of up to 2.75 m (e.g., FP-A) indicates that flows often extended along conduits that varied considerably in size and encompassed a large number of fractures (Figure 10). This observation of flow paths inclusive of many fractures is particularly important because: (1) it suggests that flow in this fractured rock is not restricted to sections of individual fractures, and (2) water flowing along these flow paths is in contact with a large surface area associated with multiple fractures. An accurate assessment of the fracture–matrix interface area (or effective matrix-diffusion coefficient) is required for evaluating the transport of dissolved radionuclides and radioactive colloids in both unsaturated and saturated fractured rock [e.g., *Bodvarsson et al*., 2001; *Neretnieks*, 1980, 2002]. If this area is assumed to include only that area wetted by focused flow along fracture surfaces, it is

much smaller than the area wetted along the observed flow zones, resulting in significant underestimation of the extent of matrix diffusion. Thus, the flow-rate dependence of fracture-matrix interactions requires more experimentally based quantification.

The range (i.e., a factor of 3) for the apparent velocities of the wetting fronts (0.25 to 0.74 m/day) suggests that as water moved through the formation, wetting the matrix and/or material on the surface of fractures, it was subject to similar flow impediments. The initial, relatively slower migration likely transitioned to faster flow velocities of 2-40 m/day, similar to those measured by *Tokunaga and Wan* [1997] when they investigated matric film flow along a block of Bishop Tuff. One interesting anomaly in the velocity profile was the location of the fast flow zone furthest (laterally) from the infiltration pond, whereas the flow path located immediately below the infiltration pond was about twice as slow. The wetting-front velocity was apparently not correlated to the extent of flow-zone lateral divergence from the infiltration plot.

6. Conclusions

While observations from this investigation concur with previous studies in that preferential flow is a dominant process, they also suggest that existing conceptual models may be inconsistent in their representation of some fundamental aspects of water movement through unsaturated fractured rock.

Specifically,

1. Flow is not focused along a section of a large fracture; rather, it encompasses numerous fractures of various sizes. Thus, the area across which fracture-matrix

interactions occur is significantly greater than would be expected for a focused flow model.

2. Further, these flow zones do not necessarily interact. Gravity-driven vertical flow can have a significant lateral component not entirely driven by capillarity, but rather by the geometry of fracture networks.
3. Capillary barriers may not reduce flux into an excavated cavity, but rather they may increase the area through which flow could occur by diverting water from the ceiling to side walls.
4. The range in velocities for the leading edge of flow paths suggests the presence of a longitudinal dispersion currently excluded in conceptual models of flow and transport in unsaturated fractured rock.
5. References in numerical studies addressing flow and transport (on the scale of meters) often allude to laboratory studies that show intermittent flow and flow focusing in fractures. At the scale of meters, these processes/observations may be minor, and incorporating them into conceptual models could lead to erroneous conclusions

Finally, observations from this investigation suggest the need for field experiments conducted at the scale of tens of meters and at lower flow rates, to help better guide the development of conceptual models for flow and transport in fractured rock.

Acknowledgments

Preparation of graphics by Diana Swantek and review of the text by Tetsu Tokunaga, Paul Cook, and Dan Hawkes are gratefully acknowledged. This work was supported by the Director, Office of Civilian Radioactive Waste Management, U.S. Department of Energy, through Memorandum Purchase Order QA-B004220RB3X between Bechtel SAIC Company, LLC, and the Ernest Orlando Lawrence Berkeley National Laboratory (Berkeley Lab). The support is provided to Berkeley Lab through the U.S. Department of Energy Contract No. DE-AC03-76SF00098

References

Beven, K., and P. Germann (1982), Macropores and water flow in soils, *Water Resources Research, 18, 1311-1325*.

Buesch, D. C., R. W. Spengler, T. C. Moyer, and J. K. Geslin (1996), Proposed stratigraphic nomenclature and macroscopic identification of lithostratigraphic units of the Paintbrush Group exposed at Yucca Mountain, Nevada., *U.S. Geol. Surv. Open-File Report 94-46*9, Denver, Colorado.

Buesch, D. C., and R. W. Spengler (1998), Character of the middle nonlithophysal zone of the Topopah Spring Tuff at Yucca Mountain, in *Proceedings of the Eighth International Conference on High-Level Radioactive Waste Managemen*t, 1-14 May, American Nuclear Society, Las Vegas, NV.

Dahan, O., R. Nativ, E. Adar, and B. Berkowitz (1998), Measurement system to determine water flux and solute transport through fractures in the unsaturated zone, *Ground Water*, 36, 444-449.

Fabryka-Martin, J. T., P. R. Dixon, S. Levy, B. Liu, H. J. Turin, and A. V. Wolfsburg (1996), Summary report of Chlorine-36 studies: Systematic sampling for Chlorine-36 in the Exploratory Studies Facility, *Los Almos National Laboratory*

Milestone Report 3783AD, Los Alamos National Laboratory, Los Alamos, New Mexico.

Flint, L. E. (1998), Characterization of hydrogeologic units using matrix properties, Yucca Mountain, Nevada, *U.S. Geological Survey Water Resources Investigations Report* 97-4243, 64 pp.

Hillel, D. E., and J. Y. Parlange (1972), Wetting front instability in layered soils, *Soil Sci. Soc. Am. Proc.* 36, 697-702.

Hinds, J. J., G. S. Bodvarsson, and G. H. Nieder-Westermann (2003), Conceptual evaluation of the potential role of fractures in unsaturated processes at Yucca Mountain, *Journal of Contaminant Hydrology*, 62-63, 111-132.

Nicholl, M. J., R. J. Glass, and S. W. Wheatcraft (1994), Gravity-Driven infiltration instability in initially dry nonhorizontal fractures, *Water Resources Research*, 30, 2533-2546.

Paces, J. B., L. A. Newmark, B. D. Marshall, J. F. Whelan, and Z. E. Peterman (1996), Ages and origins of subsurface secondary minerals in the Exploratory Studies Facility, *1996 Milestone Report 3GQH450M*, U.S. Geological Survey, Denver, Colorado.

Pruess, K. (1996), A Fickian diffusion model for the spread of liquid plumes infiltrating in heterogeneous media, *Transport in Porous Media*, 24, 1-33.

Pruess, K., B. Faybishenko, and G. S. Bodvarsson (1999), Alternative concepts and approaches for modeling flow and transport in thick unsaturated zones of fractured rock, *Journal of Contaminant Hydrology*, 38, 281-322.

Roth K., (1995), Steady state flow in an unsaturated, two-dimensional, macroscopically homogeneous, miller-similar medium, *Water Resources Researc, 31, 2127-2140.*

Salve, R., J. S. Y. Wang and T. K. Tokunaga (2000), A probe for monitoring wetting front migrations in rocks, *Water Resources Research.* 36, 1359-1367.

Simunek, J., N. J. Jarvis, M. Th. van Genuchten, and A. Gardenas (2003), Review and comparison of models for describing non-equilibrium and preferential flow and transport in the vadose zone, *Journal of Hydrology*, 272, 14-35.

Su, G., J. T. Geller, K. Pruess, and F. Wen, (1999), Experimental Studies of water seepage and intermittent flow in unsaturated, rough walled fractures, *Water Resources Research*, 35, 1019-1037.

Thordarson, W. (1965), Perched groundwater in zeolitized-bedded tuff, Rainier Mesa and vicinity, Nevada Test Site, Nevada, *U.S. Geological Survey Report TEI-862,* 93 pp.

Tokunaga, T. K., and J. Wan (1997), Water film flow along fracture surfaces of porous rock *Water Resources Research,* 33, 1287-1295.

Tokunaga, T. K., and J. Wan (2001), Surface-zone flow along unsaturated rock fractures, *Water Resources Research,* 37, 287-296.

Trautz R. C., and J. S. Y. Wang (2002), Seepage into an underground opening constructed in unsaturated fractured rock under evaporative conditions, *Water Resources Research,* 38, 1188, doi:10.1029/2001WR000690.

Wood, T. R., and G. T. Norrell (1996), Integrated large-scale aquifer pumping and infiltration test, Groundwater Pathways OU 7-06, *Summary Report, INEEL-96/0256,* Lockheed Martin Idaho Technologies, ID.

Figure Captions

Figure 1. (A) Location of Yucca Mountain; (B)Three-dimensional view of the test bed in the Exploratory Studies Facility at Yucca Mountain - the test bed is located at the crossover point of the two tunnels i.e., the Main Drift and the Cross Drift; (C) Location of the infiltration plot along the floor of Alcove 8; and (D) Location of monitoring boreholes around Niche 3.

Figure 2. (A) Photograph of infiltration zone in Alcove 8 showing subplots and permeameters that were used to supply water; (B) Cumulative infiltration (solid line) and daily infiltration rates measured over the entire infiltration plot.

Figure 3. (A) Design of electrical resistance probes (ERPs) used to monitor saturation changes along boreholes; and (B) Location of ERPs along trays installed in boreholes.

Figure 4. (A) Plan view showing location of infiltration plot relative to monitoring boreholes surrounding Niche 3. Numbers indicate the location along the boreholes where various wetting fronts were detected. The letters A-H indicated the location of flow zones defined by wetting front velocity and location. (B) End view of Niche 3 showing the flow zones intercepted by BH4, BH7, and BH9, located along the same vertical plane.

Figure 5. Arrival of wetting fronts in the vicinity of Niche 3 associated with (A) FP-A, (B) FP-B, (C) FP-C, and (D) FP-D. These are four of the six large flow paths (i.e., A-G in

Table 1). The 'x' axis starts at the time infiltration began (i.e., on August 20, 2002). The 'Y' axis has the resistance measured at each location along the boreholes. A decreasing resistance indicates wetting.

Figure 6. Plot of resistance measurements along the length of BH3 showing two distinct flow paths (FP-E and FP-H) intercepted by the borehole.

Figure 7. Saturation changes measured close to the walls of Niche 3. Data shown is for the six boreholes, with each color representing a separate borehole. Note that the legend includes the borehole number and sensor location along the borehole.

Figure 8. Development of lateral flow along the back wall of Niche 3 over a period of 24 hours. This wetting likely occurred as water diverted from the ceiling migrated through the formation close to the walls. Circles indicate the location of changes.

Figure 9. Saturation changes with specific flow paths after initial wetting for the duration of ponded infiltration. Note that for two weeks in February 2003, no data was collected due to datalogger problems.

Figure 10. Water emerging along a network of fractures along the back wall of Niche 3. The tube in the lower right-hand corner had an outer diameter of 1 cm. This photograph shows that flow in this fractured rock is through a network of fractures generally less than 1 m in length.

Table 1. Details of discrete flow paths that developed as ponded water was released along fractured welded tuff (See Figure 3)

Wettting Front[1]	Location		Width	Travel Time	Velocity	Flow Path	Extent of lateral spread[3]
	Borehole ID[2]	Depth (m)	(m)	(days)	(m/day)		(m)
1	BH4	3.40-5.90	2.75	31	0.74	A	4.75
2	BH7	0.65-0.90	0.50	32	0.73	A	
3	BH7	2.15-2.65	0.75	32	0.72	A	
4	BH4	2.4	0.25	33	0.69	B	
5	BH9	8.4	0.25	29	0.68	B	
6	BH7	0.15-0.40	0.50	33	0.67	B	
7	BH4	0.15-0.40	0.50	35	0.67	B	
8	BH10	7.65-8.90	1.50	31	0.65	B	1.25
9	BH4	2.65-2.90	0.50	36	0.64	B	
10	BH4	3.15	0.25	38	0.60	B	
11	BH4	2.15	0.25	39	0.59	B	
12	BH9	8.15	0.25	36	0.56	B	
13	BH5	1.65	0.25	43	0.54	I	1.25
14	BH9	7.65-7.90	0.50	38	0.52	B	
15	BH3	0.15-0.40	0.50	45	0.51	CD	
16	BH2	0.15-2.40	2.50	46	0.50	C	1.2
17	BH5	1.9	0.25	48	0.48	G	2.5
18	BH3	0.65-1.40	1.00	50	0.46	H	
19	BH10	5.65	0.25	46	0.43	D	0
20	BH10	3.40-5.15	2.00	47	0.43	D	
21	BH3	3.15-3.90	1.00	58	0.40	E	3.1
22	BH6	0.15-0.40	0.50	60	0.38	CD	
23	BH5	0.15-0.65	0.75	62	0.37	CD	
24	BH6	0.65-3.15	2.75	91	0.25	F	1.2

[1]Wetting Front as identied in Figure

[2]Boreholes location is presented in Figure 1

[3] Horizontal distance to center of flow

Table 1. Features of flow paths identified along boreholes surrounding Niche 3

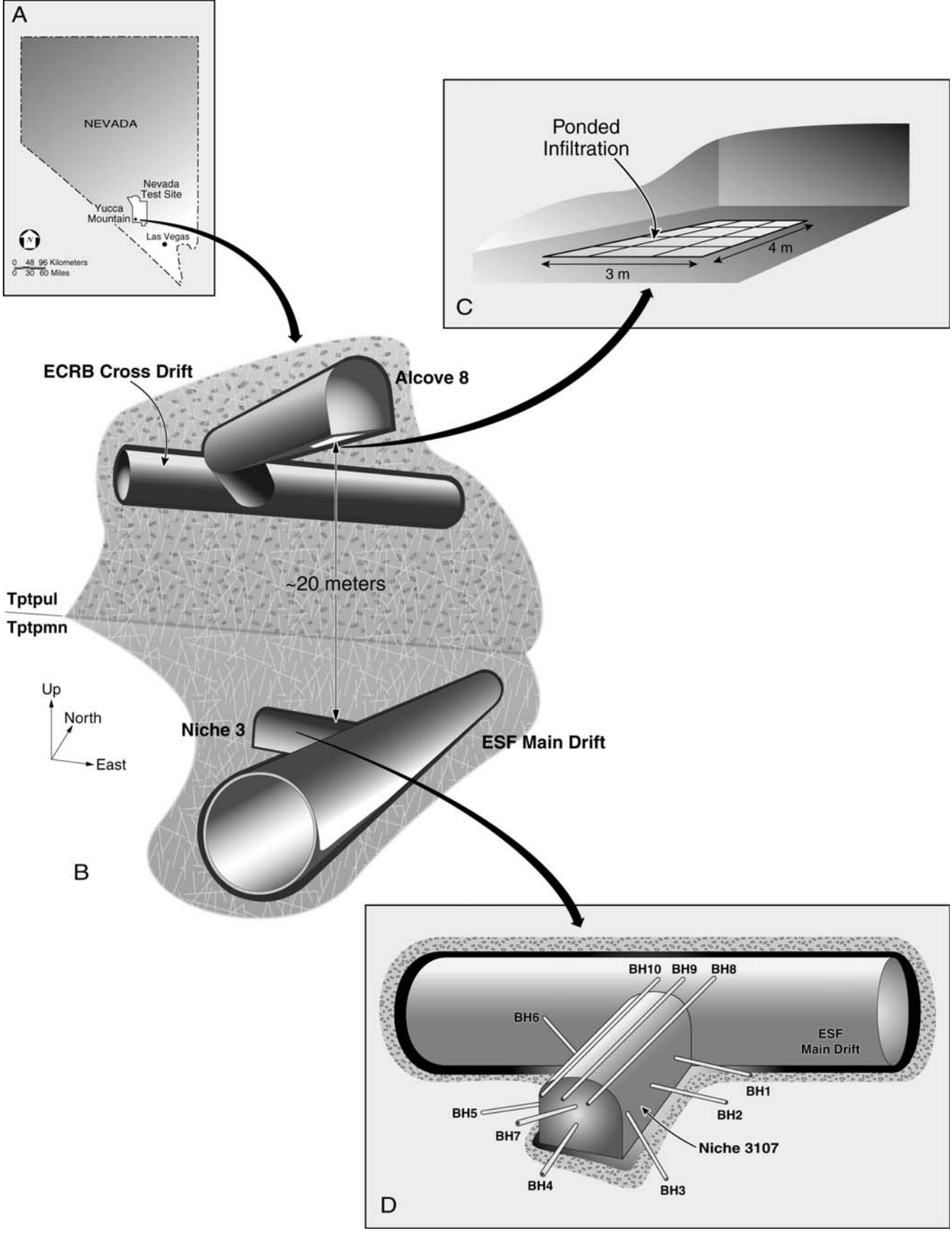

Figure 1. (A) Location of Yucca Mountain: (B)Three-dimensional view of the test bed in the Exploratory Studies Facility at Yucca Mountain. the test bed is located at the crossover point of the two tunnels i.e., the Main Drift and the Cross Drift; (C) Location of the infiltration plot along the floor of Alcove 8; and (D) Location of monitoring boreholes around Niche 3.

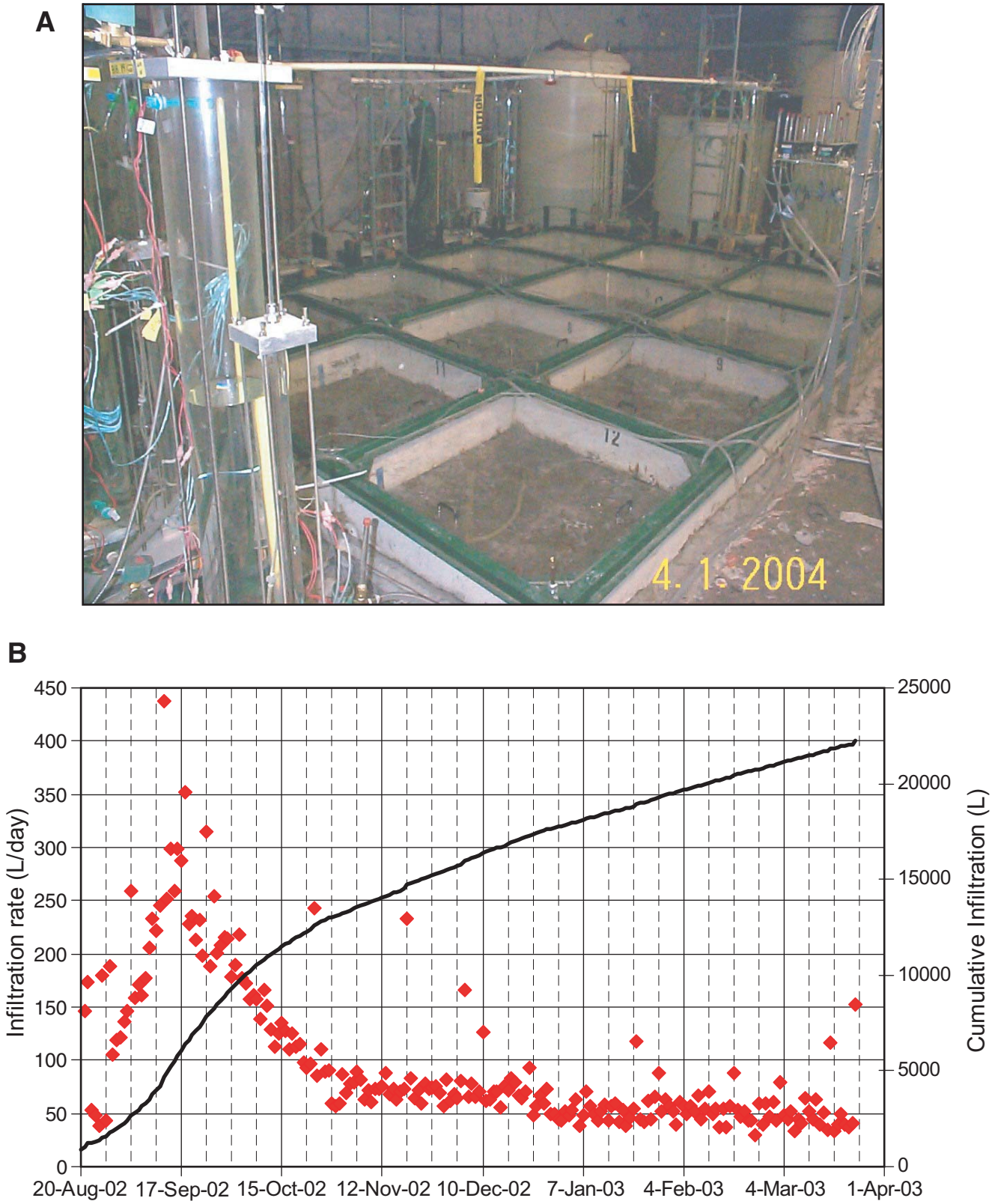

Figure 2. (A) Photograph of infiltration zone in Alcove 8 showing subplots and permeameters that were used to supply water; (B) Cumulative infiltration and daily infiltration rates measured over the entire infiltration plot.

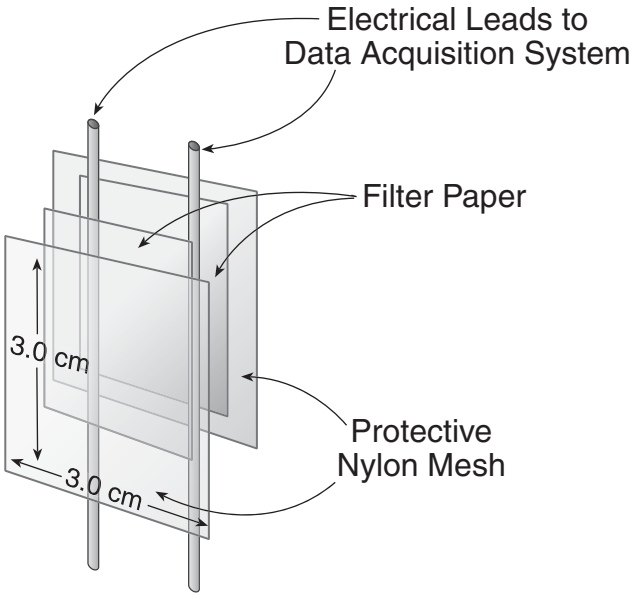

(a) Electrical Resistivity Probes used in Borehole Measurements

(b) Borehole Sensor Tray with ERP –
Oblique View

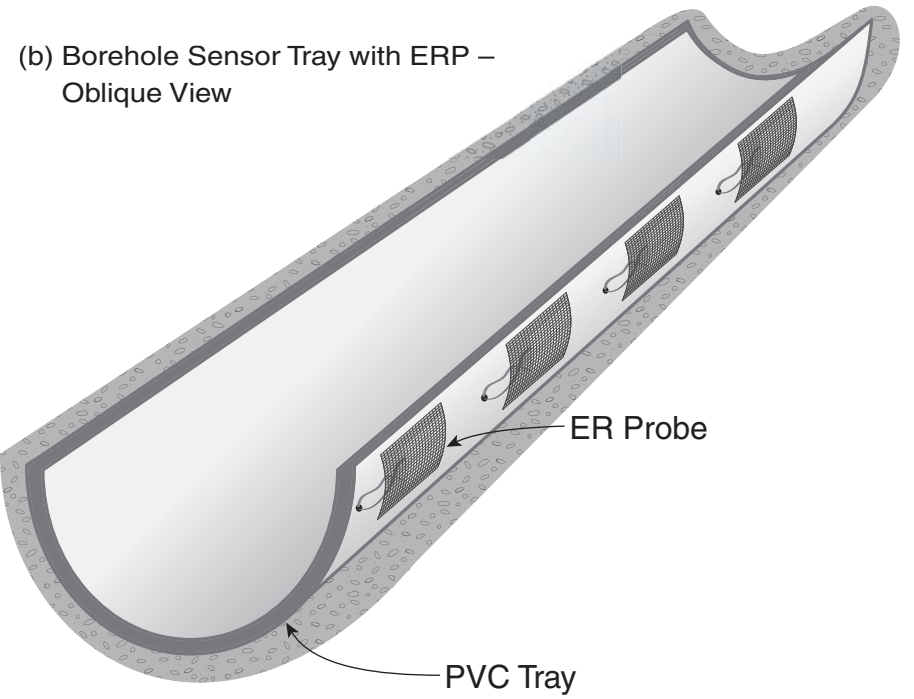

Figure 3. (A) Design of electrical resistance probes (ERPs) used to monitor saturation changes along Boreholes; and (B) Location of ERPs along trays installed in boreholes

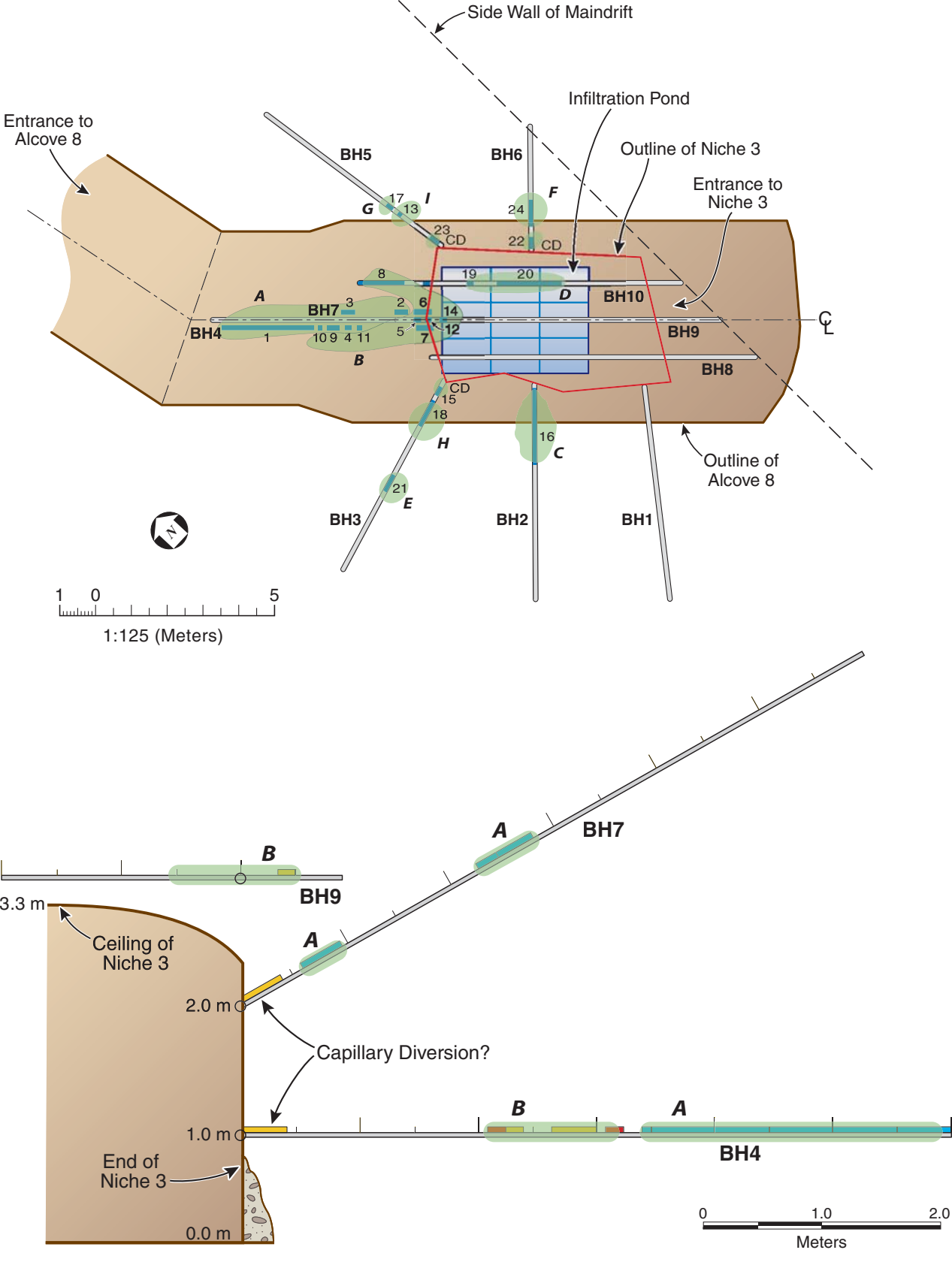

Figure 4. (A) Plan view showing location of infiltration plot relative to monitoring boreholes surrounding Niche 3. Numbers indicate the location along the boreholes where various wetting fronts were detected. The letters A-H indicated the location of flow zones defined by wetting front velocity and location. (B) End view of Niche 3 showing the flow zones intercepted by BH4, BH7 and BH9, which were located along the same vertical plane.

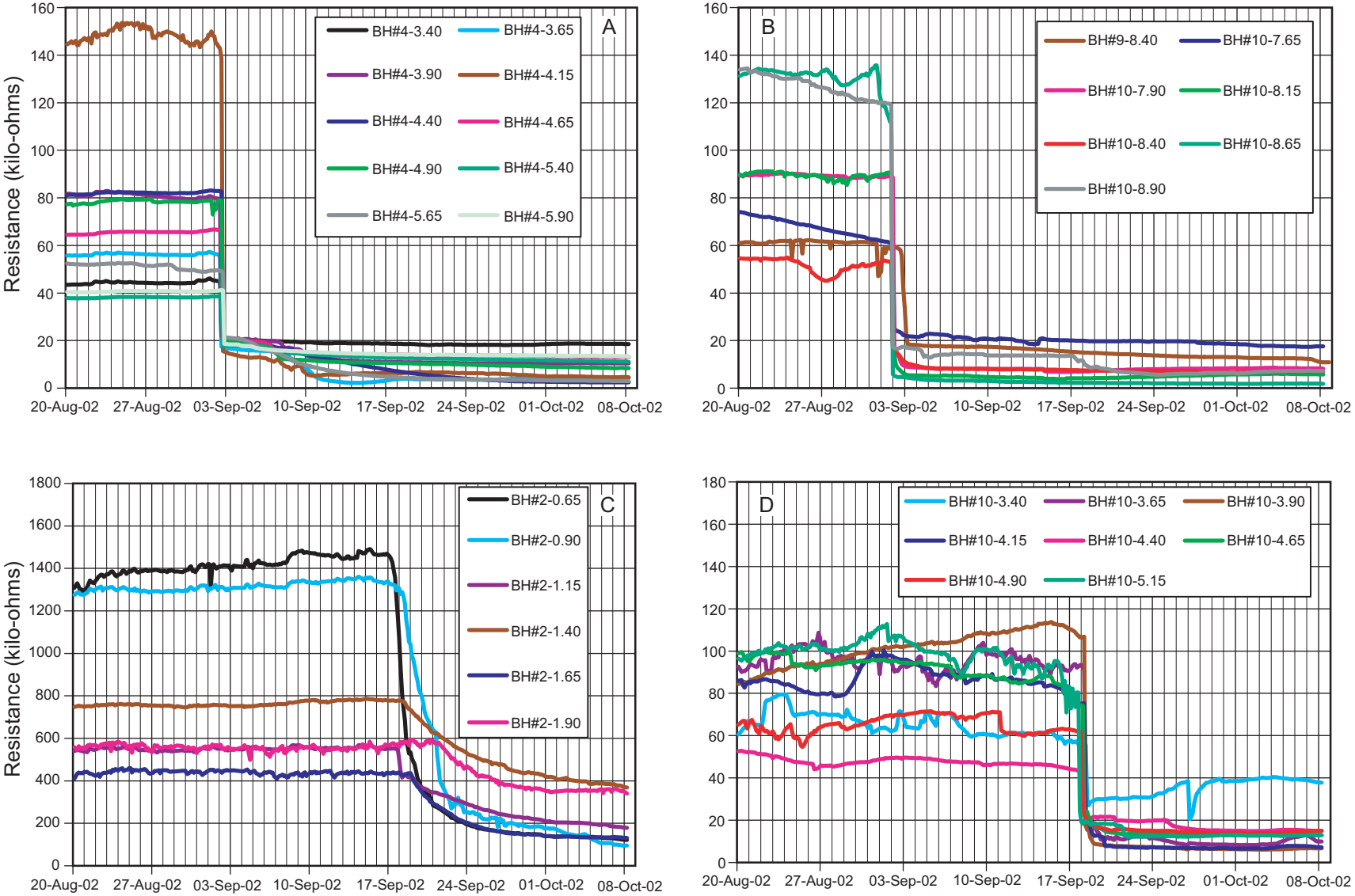

Figure 5. Arrival of wetting fronts in the vicinity of Niche 3 associated with (A) FP-A, (B) FP-B, (C) FP-C, and (D) FP-D. These are four of the six large flow paths (i.e., A-G in Table 1). The 'x' axis starts at the time infiltration began (i.e., on August 20, 2002). The 'Y' axis has the resistance measured at each location along the boreholes. A decreasing resistance indicates wetting.

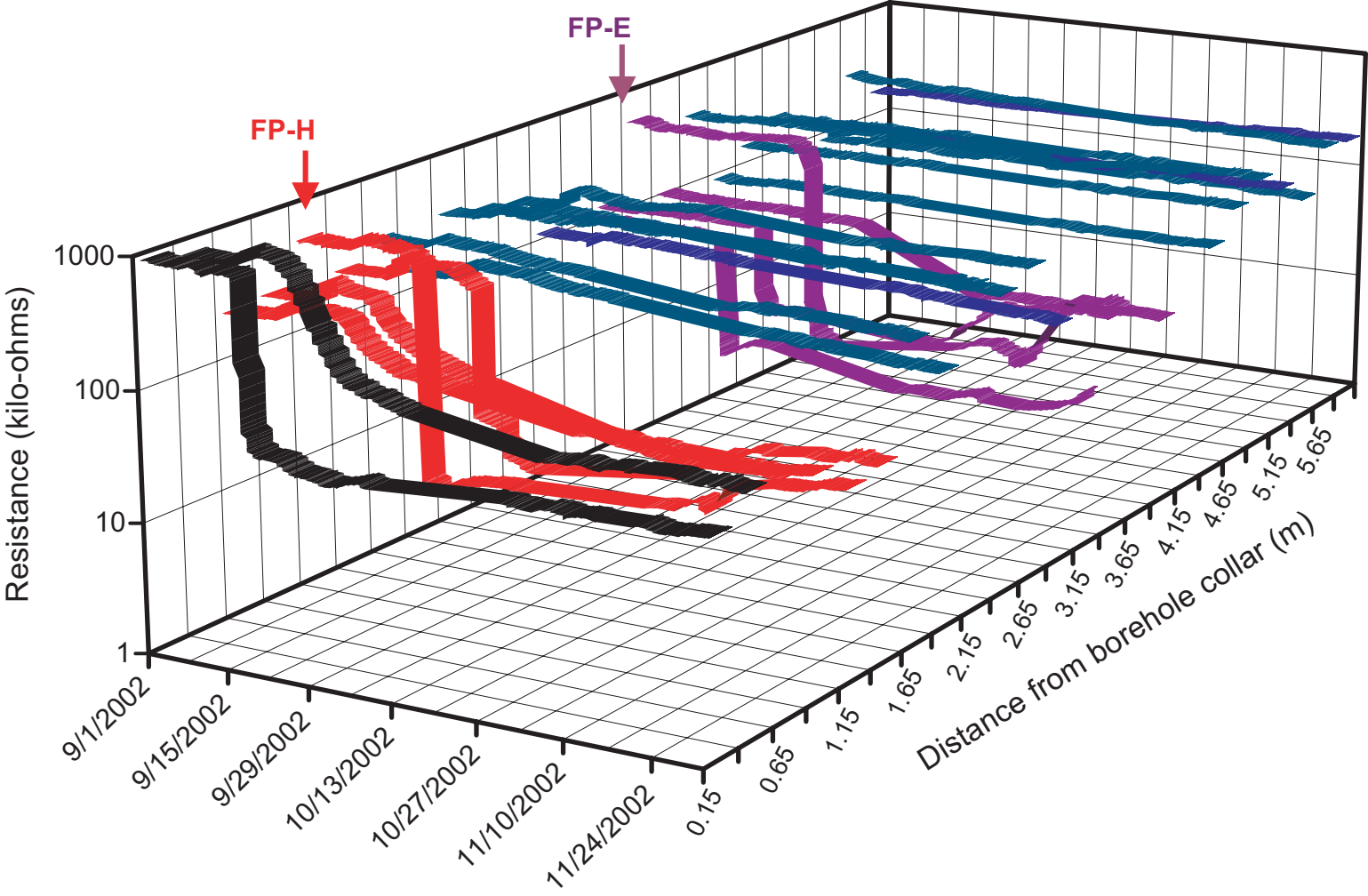

Figure 6. Plot of resistance measurements along the length of BH3 showing two distinct flow paths (FP-E and FP-H) that were intercepted by the borehole.

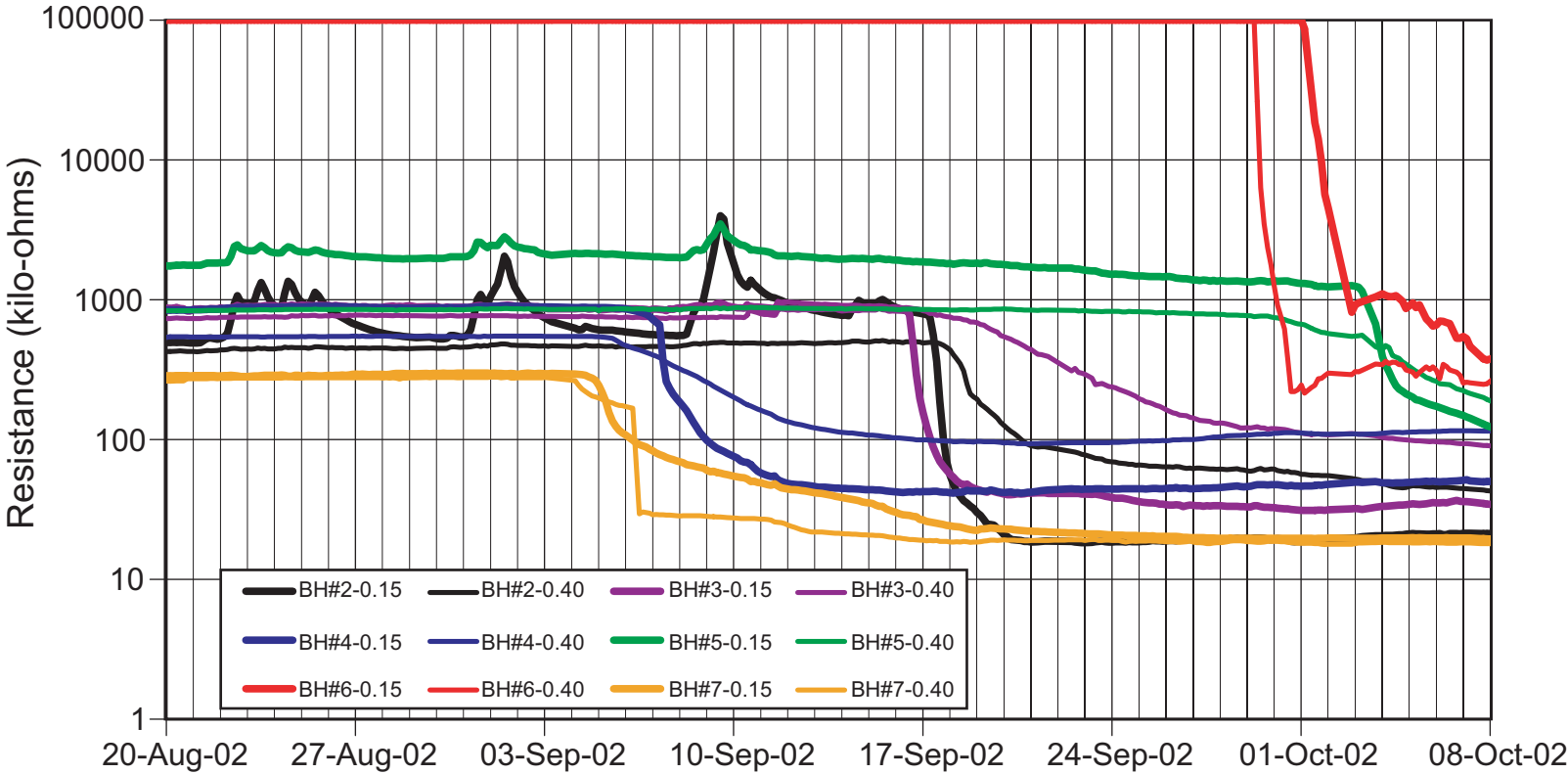

Figure 7. Saturation changes measured close to the walls of Niche 3. Data shown is for the six boreholes with each color representing a separate borehole. Note the legend includes the borehole number and location of sensor along the borehole.

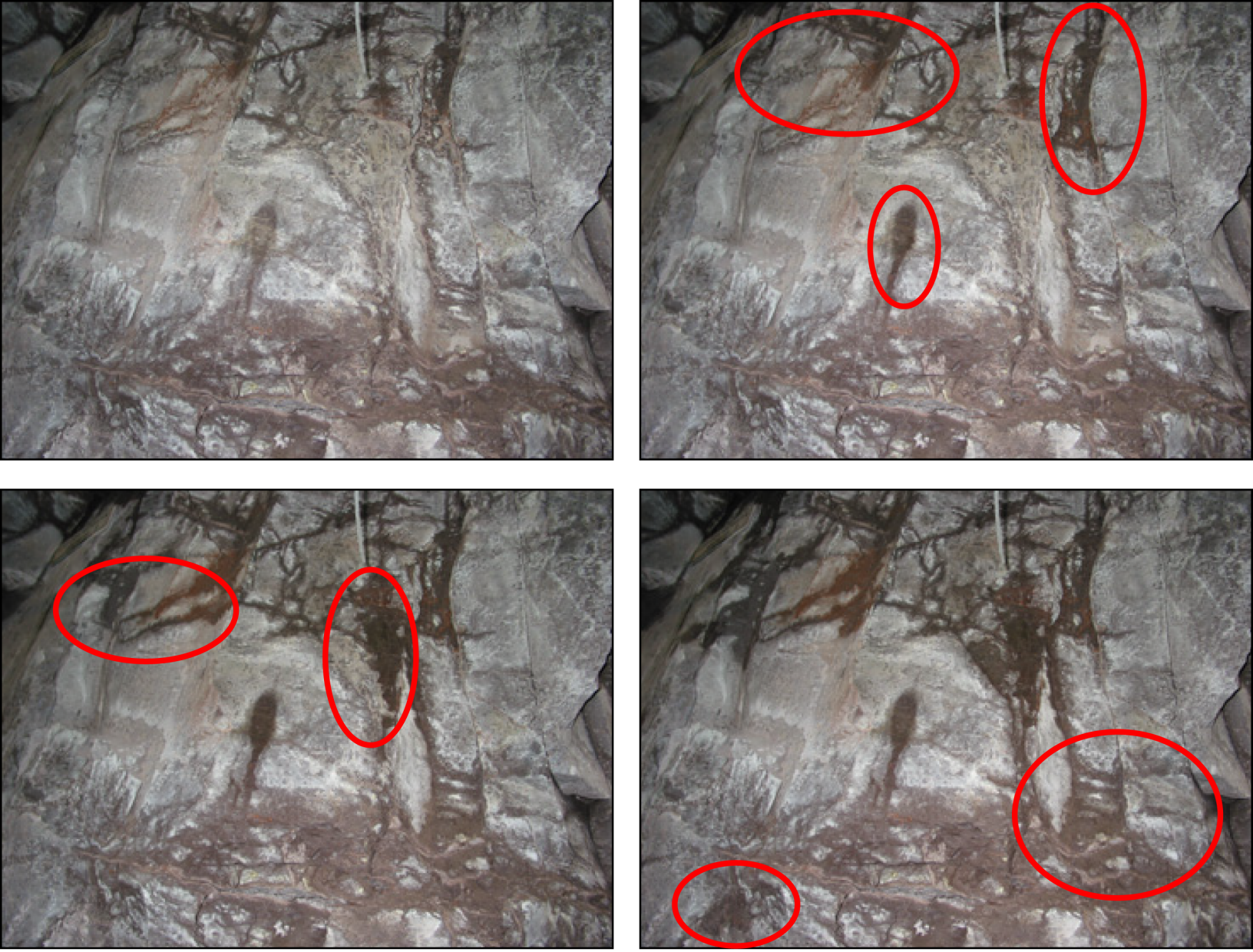

Figure 8. Development of lateral flow along the back wall of Niche 3 over a period of 24 hours. This wetting likely occurred as water was diverted from the ceiling migrated through the formation close to the walls. Circles indicate the location of changes.

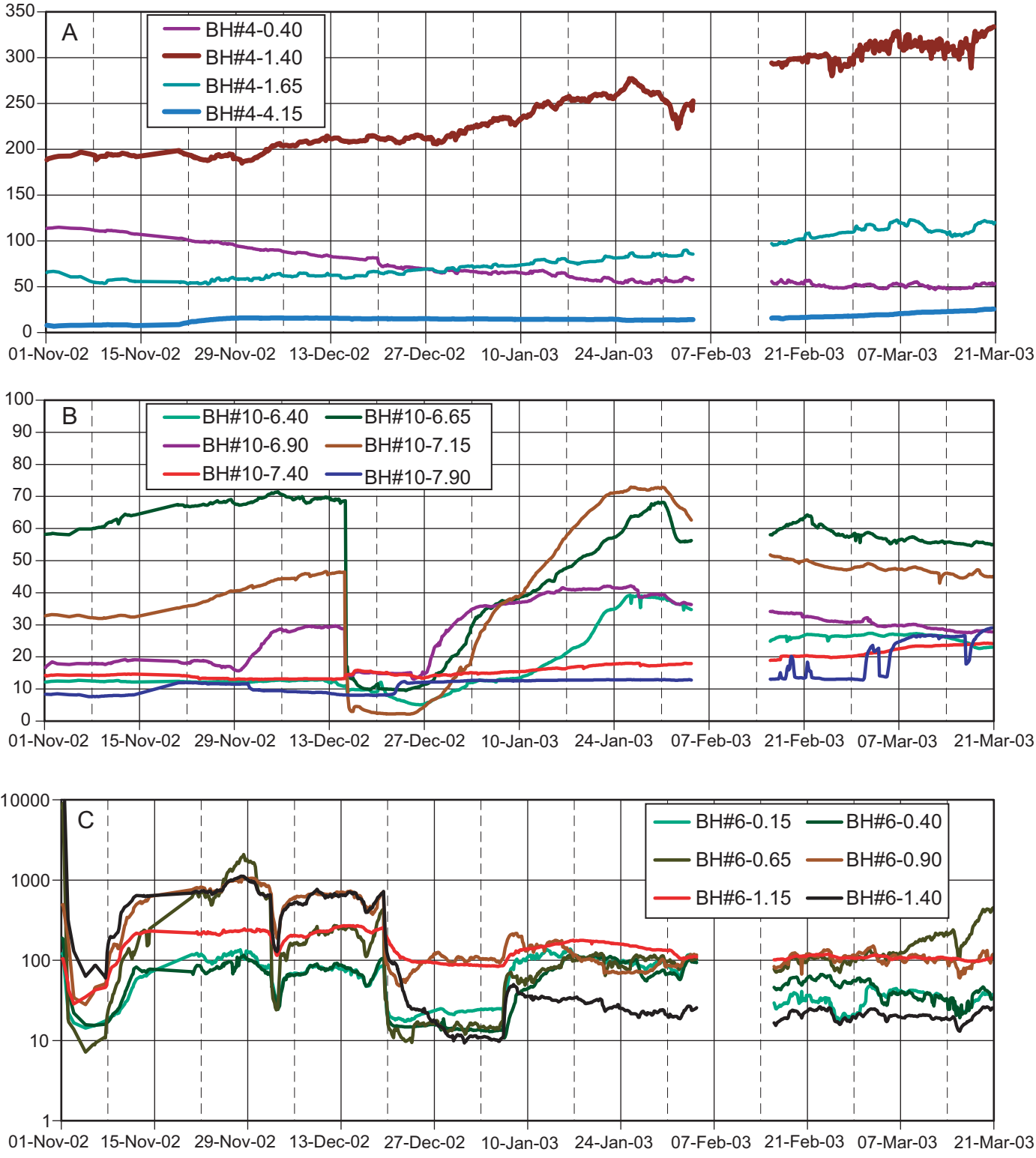

Figure 9. Saturation changes with specific flow paths after initial wetting for the duration of ponded infiltration. Note that for two weeks in February 2003 no data was collected due to datalogger problems.

Figure 10. Water emerging along a network of fractures along back wall of Niche 3. The tube in the lower right hand corner had an outer diameter of 1 cm. This photograph shows that flow in this fractured rock is through a network of fractures which is largely made up of fractures which are less than 1m in length.

Wettting Front[1]	Location		Width	Travel Time	Velocity	Flow Path	Extent of lateral spread[3]
	Borehole ID[2]	Depth (m)	(m)	(days)	(m/day)		(m)
1	BH4	3.40-5.90	2.75	31	0.74	A	4.75
2	BH7	0.65-0.90	0.50	32	0.73	A	
3	BH7	2.15-2.65	0.75	32	0.72	A	
4	BH4	2.4	0.25	33	0.69	B	
5	BH9	8.4	0.25	29	0.68	B	
6	BH7	0.15-0.40	0.50	33	0.67	B	
7	BH4	0.15-0.40	0.50	35	0.67	B	
8	BH10	7.65-8.90	1.50	31	0.65	B	1.25
9	BH4	2.65-2.90	0.50	36	0.64	B	
10	BH4	3.15	0.25	38	0.60	B	
11	BH4	2.15	0.25	39	0.59	B	
12	BH9	8.15	0.25	36	0.56	B	
13	BH5	1.65	0.25	43	0.54	I	1.25
14	BH9	7.65-7.90	0.50	38	0.52	B	
15	BH3	0.15-0.40	0.50	45	0.51	CD	
16	BH2	0.15-2.40	2.50	46	0.50	C	1.2
17	BH5	1.9	0.25	48	0.48	G	2.5
18	BH3	0.65-1.40	1.00	50	0.46	H	
19	BH10	5.65	0.25	46	0.43	D	0
20	BH10	3.40-5.15	2.00	47	0.43	D	
21	BH3	3.15-3.90	1.00	58	0.40	E	3.1
22	BH6	0.15-0.40	0.50	60	0.38	CD	
23	BH5	0.15-0.65	0.75	62	0.37	CD	
24	BH6	0.65-3.15	2.75	91	0.25	F	1.2

[1]Wetting Front as identied in Figure

[2]Boreholes location is presented in Figure 1

[3] Horizontal distance to center of flow

Table 1. Features of flow paths identified along boreholes surrounding Niche 3